Research Article

UPLC-Q-Exactive Orbitrap-MS Analysis of *Anchusa italica* Retz. Flowers: Molecular Docking, Dynamics Modeling, and Pharmacokinetics for Cardiovascular Disease

¹Linvang Wang, ²Yan Chen, ³Ainiwaer Aikemu and ¹Shuge Tian

Received: 11-01-2025 Revised: 10-04-2025 Accepted: 22-04-2025

Corresponding Author: Shuge Tian College of Traditional Chinese Medicine, Xinjiang Medical University, Urumqi, Email:

tianshuge@xjmu.edu.cn

Abstract: This study builds on prior UPLC-Q-Exactive Orbitrap-MS analyses of Anchusa italica Retz. Flowers (Airfs) to explore their anti-cardiovascular mechanis ms and key bioactive markers. UPLC-Q-Exactive Orbitrap-MS identified 30 major compounds, including polyphenols and flavonoids with strong antioxidant activity. The potential active ingredients were then screened using Lipinski's rule of five, and a network pharmacology method was employed to construct an 'active ingredient-target' network diagram, resulting in the identification of 28 core targets. GO and KEGG enrichment analyses were then used to reveal the potential mechanisms of these compounds in cardiovascular diseases. Molecular docking experiments demonstrated that 5-hydroxy-7methoxy-3-(4-hydroxybenzylidene)chroman-4-one (HY-N8673) and caffeic acid exhibited strong binding affinity with epidermal growth factor receptor (EGFR) and SRC proteins. Molecular dynamics simulations further validated the binding stability of these compounds to the target proteins. Additionally, ADMET parameter predictions indicated that these compounds possess favorable pharmacokinetic properties and a low risk of toxicity. In conclusion, this study provides a scientific basis for the application of Airfs in the treatment of cardiovascular diseases.

Keywords: Anchusa italica Retz. Flowers, Cardiovascular Disease, Network Pharmacology, Molecular Docking, Dynamics Modeling

Introduction

Cardiovascular disease is a major cause of mortality and disability on a global scale. Its pathogenesis is intricate, involving numerous pathophysiological processes. In recent years, with the advancement of research in the field of natural medicines, a growing number of studies highlight the cardiovascular protective potential of plant extracts and their active compounds. Anchusa italica Retz. belongs to the Boraginaceae family and is recognized as a perennial herbaceous plant (Chen et al., 2017). It is rich in flavonoids and polyphenols (Hu et al., 2020). It has anti-inflammatory, antioxidant and antimicrobial properties (Khomsi et al., 2022). Airfs are incorporated into various prescription formulations, notably "Aioweixin Oral Liquid" and "Jianxin Hemiergaoziban Anbire Tablet. The employment of UPLC-Q-Exactive Orbitrap-MS for preliminary characterisation and initial quantification of chemical constituents, in conjunction with network pharmacology and molecular docking, has emerged as an effective methodology for elucidating the mechanisms of drug constituents in the treatment of diseases (Shu et al., 2024; Jiang et al., 2024).

The objective of the present study was to ascertain the mechanism of action of Airfs in the treatment of cardiovascular diseases. This accomplishment was made through the application pharmacology, molecular docking, molecular dynamics simulation, and ADMET toxicity prediction. These methods were utilized in conjunction with the results obtained from Airfs detected via UPLC-Q-Exactive Orbitrap-MS. The study also sought to provide references for the development and safety of the drug.

Materials and Methods

UPLC-Q-Exactive Orbitrap-MS Methodology and Data Collection

The methodology for ultra-performance liquid chromatography coupled with high-resolution mass spectrometry (UPLC-Q-Exactive Orbitrap-MS) was adopted from our previous work on Anchusa italica Retz. flowers (Wang et al., 2024).

Briefly, dried flower samples were extracted with a cold solvent mixture of water, acetonitrile, and isopropanol (1:1:1, v/v/v). The extracts were centrifuged,



 $^{^{1}}$ College of Traditional Chinese Medicine, Xinjiang Medical University, Urumqi, China

²College of Medicine, Jiaxing University, Jiaxing, China

³Xinjiang Key Laboratory, Hetian Characteristic Chinese Traditional Medicine Research, Hetian, China

and the supernatant was vacuum-dried. The residue was reconstituted in 30% acetonitrile for analysis.

Chromatographic separation was achieved on a Waters HSS T3 column (100×2.1 mm, 1.8 µm) maintained at 40 °C. The mobile phase consisted of (A) 0.1% formic acid in water and (B) 0.1% formic acid in acetonitrile, with a flow rate of 0.3 mL/min. The gradient elution program was as follows: 0% B at 0-1 min, increasing to 95% B at 12 min, held until 13 min, and then returned to initial conditions for re-equilibration.

Mass spectrometric analysis was conducted with a heated electrospray ionization (HESI) source in both positive and negative ionization modes. The full MS/dd-MS² data-dependent acquisition was used with the following parameters:

• Mass range: 70-1050 Da

• Spray voltage: +3.0 kV / -2.8 kV

• Full MS resolution: 70,000

• MS/MS resolution: 17,500

Raw data were processed using Progenesis QI software (Waters Corporation) for peak alignment, normalization, and compound identification. Metabolite identification was based on accurate mass and MS/MS fragmentation matching against commercial and custom databases, with a minimum spectral match score of 0.7.

Screening and Target Prediction of the Main Active Ingredients of Anchusa italica Retz. Flowers

The identification of the compounds was followed by a screening process for relative content using UPLC-Q-Exactive Orbitrap-MS for compounds with a relative content greater than 0.2%. The evaluation of the compounds was then conducted by integrating the TCMSP (Traditional Chinese Medicine Systematic Pharmacology Database and Analysis Platform) database using SwissTarget Prediction in accordance with the Lipinski's fivefold rule. The evaluation of the compounds by SwissTarget Prediction according to the Lipinski's five-fold rule resulted in the identification of 30 eligible compounds, TCMSP, and the SwissTarget Prediction database (Liu et al., 2024). Subsequently, the PubChem database was employed to identify the SMILES structure of the active ingredients. The SMILES structure of the ingredient active was input into SwissTargetPrediction database to predict the target points of the ingredients. The results of the screening are merged to remove duplicates. In order to identify disease targets related to cardiovascular disease, the OMIM database, GeneCards database (score ≥ 5), and TTD database were consulted. The targets were then combined and de-emphasized in order to obtain disease targets.

Network Diagram Construction

WeiShengXin was employed to identify the intersection of disease targets and compound targets. The

resulting targets were imported into the String database, where a confidence level of >0.7 was set for scoring. Targets that were not connected were concealed, and inter-target interactions were identified. The data were then imported into the Cytoscape 3.10.0 software, where protein-protein interactions were constructed. The network analyzer was employed to calculate the degree value, and the 28 core targets were filtered out with the limit of 2 times the median degree value (Gong *et al.*, 2023; Santos *et al.*, 2022). A network diagram of the "active ingredient targets" was constructed.

Enrichment Analysis

Go and Kegg analyses were performed using the microbiology platform, and the analysis module integrated R language packages such as clusterProfiler and pathview. Data were screened at P-value ≤ 0.05 , and GO analysis was applied to the first 10 entries of each item, which were imported into the microbiology platform for visualization. KEGG was applied to the first 20 pathways for visualization and analysis (Gajera *et al.*, 2024).

Docking of Molecules

Docking was performed using the LibDock module in Discovery Studio 3.0. Protein identification was conducted via the UniProt database. The PDB number should then be copied and the PDB database accessed to download the 3D files (.sdf) of the desired proteins. The Pubchem database ought to be utilized for locating the 3D files pertaining to the core components. The next step is to open Discovery Studio (DS) software and process each protein molecule in order to remove water molecules, ligands, and complementary residues in preparation for docking. To process all compounds, select "Prepare Ligands" from the small molecule menu bar within the DS software. Each protein should be defined as a receptor molecule, and the machine learning module should be used to predict the possible binding regions. In the event that the crystal structure does not include H atoms, the receptor should be hydrogenated prior to this step. Subsequently, the processed compounds are docked with multiple compounds using the "Receptor-Ligand Interactions" module, and the corresponding parameters are set. The docking results are then output and analyzed at the conclusion of the program. Observations indicate that a higher docking score corresponds to stronger binding activity between the ligand compound and the receptor (Xiang et al., 2024).

Molecular Dynamics Simulation

All-atom molecular dynamics simulations were performed on the basis of the small molecule-protein complexes obtained by docking as initial structures, using AMBER 22 software (Salomon-Ferrer *et al.*, 2013). Prior to the simulation, the charge of the small molecule was calculated by antechamber module and

Hartree-Fock (HF) SCF/6-31G* of Gaussian 09 software. Subsequently, the small molecules and proteins were described using the GAFF2 small molecule force field and the ff14SB protein force field, respectively (Wang *et al.*, 2005). The LEaP module was utilised for each system to add hydrogen atoms, a truncated octahedral TIP3P solvent box was added to the system at a distance of 10 Å (Linse & Hub, 2021), to balance the system charge, Na+/Cl- was introduced. Ultimately, the topology and parameter files necessary for the simulations were generated.

Molecular dynamics simulations were conducted using AMBER 22 software. Before commencing the simulations, the system underwent energy optimization, specifically employing the steepest descent method for 2500 steps, followed by the conjugate gradient method for another 2500 steps. Following the completion of the energy optimisation of the system, a 200 ps warming of the system at a fixed volume and constant rate of warming was used to gradually increase the temperature of the system from 0 K to 298.15 K. An NVT (isothermal isobaric) system simulation of 500 ps was carried out to ensure the homogeneous distribution of solvent molecules within the solvent box at a constant temperature of 298.15 K. Subsequently, the system temperature was adjusted to match the temperature of the solvent box through the implementation of the NVT (isothermal isobaric) system simulation. The NPT (isothermal isobaric) simulation of the entire system was run for 500 ps to achieve equilibrium. Following this, the composite system underwent NPT (isothermal isobaric) tethered simulations for 100 ns, maintaining periodic boundedness conditions. During these simulations, the non-bond truncation distance was fixed at 10 Å, while the Particle Mesh Ewald (PME) method was employed to compute long-range electrostatic interactions. Bond lengths of hydrogen atoms were constrained using the SHAKE method, and temperature was controlled via the Langevin algorithm, with a collision frequency γ of 2 ps ¹. The pressure of the system is set to 1 atm, and the integration step is set to 2 fs, with the trajectories saved at 10 ps intervals. The trajectories are saved for subsequent analyses (Kräutler et al., 2001).

The free energies of binding between proteins and ligands for all systems were calculated by the MM/GBSA method. MD trajectories with a duration of 90-100 ns were utilised as the basis for the calculations in this study, employing the following equations:

$$egin{aligned} \delta G_{bind} &= \delta \mathrm{G}_{\mathrm{complex}} - \left(\delta \mathrm{G}_{\mathrm{receptor}} + \delta \mathrm{G}_{\mathrm{ligand}}
ight) \ \delta G_{bind} &= \delta \mathrm{E}_{\mathrm{internal}} + \delta \mathrm{E}_{\mathrm{VDW}} + \delta \mathrm{E}_{\mathrm{elec}} + \delta \mathrm{G}_{\mathrm{GB}} + \delta \mathrm{G}_{\mathrm{SA}} \end{aligned}$$

This term is used to denote internal energy, van der Waals interactions, and electrostatic interactions. The internal energies comprise the bond energy (Ebond), the angular energy (Eangle), and the torsion energy (Etorsion); collectively, these are designated as the solvation free energy. The polar solvation free energy is

denoted by GGB, and the non-polar solvation free energy by GSA. The GB model developed by Nguyen *et al.* (2013) was employed in this study (igb = 2). The non-polar solvation free energy (GSA) is then calculated based on the product of surface tension (γ) and solvent-accessible surface area (SASA), GSA = 0.0072 × SASA.Entropy change is ignored in this study due to the high consumption of computational resources and low accuracy (Genheden & Ryde, 2015; Rastelli *et al.*, 2010; Xu *et al.*, 2013).

Prediction of the ADMET Parameters

The ADMET parameters were predicted using ADMET lab 2.0 (Xiong *et al.*, 2021). In addition, we also calculated the drug-likeness of compounds. Druglike properties were assessed base on the prediction of Lipinski's 'rule of 5', including molecular weight, log P value, number of hydrogen bonds donor, and acceptor.

Results

Identification of the Compounds in Anchusa italica Retz. Flowers

The outcomes of the identification process were methodically arranged, and the substances were categorised according to their potency. Substances that ranked within the top 30% were then subjected to further scrutiny. The results of this analysis can be found in Table 1 and Table 2. The main compounds were polyphenols, flavonoids and other substances with strong antioxidant activity.

Network Pharmacologic Results of Anchusa italica Retz. Flowers in the Treatment of Cardiovascular Disease

Target Prediction and Network Diagram Construction

The active ingredients were evaluated in accordance with Lipinski's five-fold rule, wherein the molecular weight of the compounds was less than 500 daltons, the number of hydrogen bond donors (including hydroxyl, amino, etc.) in the structure of the compounds was not more than 5, the number of hydrogen bond acceptors in the compounds was not more than 10, and the logarithmic value of the lipid-water partition coefficient (log P) of the compounds was between -2 and 5 (Lohit et al., 2024; Murugan et al., 2024). A total of 30 compounds met the requisite criteria, with 2,382 intersections between disease targets and 125 intersections between targets. Figure 1 illustrates the Wayne diagram, protein interaction network, component target network. The components that comply with Lipinski's law of five-fold multiplicity, possess a clear target, and are part of the core target are subjected to the "active ingredient action target" analysis. The active ingredients are listed in Table 3.

Table 1: UPLC-Q-Orbitrap-MS data information (Part A)

No.	Metabolite	Mode	e Adducts	Mass Error (ppm)	InChiKeys	Class
1	3-(3,4-Dihydroxyphenyl) lactic acid	neg	M-H, 2M-H, M- H ₂ O-H	-0.316308832	PAFLSMZLRSPALU- UHFFFAOYSA-N	Phenylpropanoic acids
2	Rosmarinate acid	neg	2M-H	7.600916835	DOUMFZQKYFQNTF- WUTVXBCWSA-N	Polyphenols
3	Rutin	pos	M+H	-1.757341311	IKGXIBQEEMLURG- NVPNHPEKSA-N	Flavonoids
4	Narcissoside	pos	M+H	-1.80057108	UIDGLYUNOUKLBM- GEBJFKNCSA-N	Flavonoids
5	Ethyl gallate	neg	2M-H	0.754971092	VFPFQHQNJCMNBZ- UHFFFAOYSA-N	Benzene and substituted derivatives
6	Isosalvianolic acid C	neg	M+FA-H	-2.767111043	AVGRZVZQTALJJF-VURDRKPISA-N	Benzoxepines
7	5-Hydroxy-7-methoxy-3-(4-hydroxybenzylidene) chroman-4-one	neg	M-H, M+FA-H	0.971925064	CEIWQXCJVAWOKP- IZZDOVSWSA-N	Homoisoflavonoids
8	Yunnaneic acid G	neg	M-2H, M-H	7.880191191	CWAPEEAMMSAHDI- BUVRPPHQSA-N	Aryltetralin lignans
9	Malic acid	neg	М-Н	-0.753114648	BJEPYKJPYRNKOW- UHFFFAOYSA-N	Hydroxy acids and derivatives
10	$N1, N5, N10\text{-}(E)\text{-}tri\text{-}p\text{-}coumaroyl spermidine}$	pos	M+H	-2.336608514	PFDVWJCSCYDRMZ- AUCPOXKISA-N	Cinnamic acids and derivatives
11	10-O-Coumaroyl-10-O-deacetylasperuloside	neg	M+FA-H	3.449770472	JXFDBOBLMXBLDZ- ULUBWVSDSA-N	Cinnamic acids and derivatives
12	Nepetin-7-glucoside	pos	M+H	-1.693115222	DMXHXBGUNHLMQO- IWLDQSELSA-N	Flavonoids
13	P-Anisic acid	neg	M-H ₂ O-H, M-H	0.332339198	ZEYHEAKUIGZSGI- UHFFFAOYSA-N	Aromatic Carboxylic Acids
14	Naringenin 7-O-gentiobioside	neg	M+FA-H	6.276315133	CSOSCFNWAYKBEH- YGEVQDKLSA-N	Flavonoids
15	Succinic acid	neg	M-H ₂ O-H, M-H, 2M-H	-1.220187467	KDYFGRWQOYBRFD- UHFFFAOYSA-N	Carboxylic acids and derivatives
16	Chrysosplenetin	neg	M-H, 2M-H, M+Cl	0.990676641	NBVTYGIYKCPHQN- UHFFFAOYSA-N	Flavonoids
17	Salvianolic acid A	neg	М-Н	-1.012712223	YMGFTDKNIWPMGF- UCPJVGPRSA-N	Stilbenes
18	L-Isoleucine	pos	M+H	-1.457240252	AGPKZVBTJJNPAG- WHFBIAKZSA-N	Carboxylic acids and derivatives
19	Ternatumoside II	neg	M-H, M+Cl	1.543633984	JAQAIBSNJJWIKR- VQMPHKDYSA-N	Flavonoids
20	Lysofungin	neg	М-Н	1.545141645	SAHCQBPGXQFTRA- ZOEHVZSMSA-N	Glycerophospholipids
21	Ailanthoidol	neg	M+Cl	-6.732557459	ZDQCRQVGMKIBPN- ONEGZZNKSA-N	2-arylbenzofuran flavonoids
22	3-Hydroxybenzoic acid	neg	M-H, 2M-H	0.455450111	FJKROLUGYXJWQN- UHFFFAOYSA-N	Benzene and substituted derivatives
23	Isosulochrin	neg	M+FA-H	1.086337199	XKIBNYJGNBTYMP- UHFFFAOYSA-N	Benzene and substituted derivatives
24	3-Acetyldeoxynivalenol	pos	M+NH ₄	-2.158535331	ADFIQZBYNGPCGY-HTJQZXIKSA N	
25	Neoeriocitrin	neg	M+FA-H	0.417576558	OBKKEZLIABHSGY- DOYQYKRZSA-N	Flavonoids
26	Caffeic acid	neg	M-H, M+Cl	0.822046551	QAIPRVGONGVQAS- DUXPYHPUSA-N	Cinnamic acids and derivatives
27	Clostebol acetate	neg	M+K-2H	3.463109522	XYGMEFJSKQEBTO- KUJXMBTLSA-N	Steroids and steroid derivatives
28	D-Tryptophan	neg	M-H, 2M-H	0.32798398	QIVBCDIJIAJPQS-SECBINFHSA-N	Indoles and derivatives
	Blumeatin B	neg	M+FA-H	1.182533103	SVPNMFZMHPLGRR- DLBZAZTESA-N	Flavonoids
30	Eugenol gentiobioside	neg	М-Н	-0.818383291	WXQNHYCVTYUIEE- OALZDZJCSA-N	Organooxygen compounds

Table 2: UPLC-Q-Orbitrap-MS data information (Part B)

No	. Metabolite	Formula	Retention time(min)	m/z	Fragment ions
1	3-(3,4-Dihydroxyphenyl) lactic acid	C ₉ H ₁₀ O ₅	2.467	197.045484	72.9931;107.0501;109.0294;122.0364;123.0451;134.0371;135.0452;151.04;179.0352;197.0455
2	Rosmarinate acid	$C_{18}H_{16}O_{8}$	6.318	719.167232	72.993;123.045;133.0296;135.0452;161.0246;179.0352;197.0457;359.0775;521.1082;719.1678
3	Rutin	$C_{27}H_{30}O_{16}$	4.184	611.159589	149.0231; 150.0307; 153.0181; 173.0597; 201.0543; 229.0493; 257.0442; 303.0495; 465.1024; 611.1588
4	Narcissoside	$C_{28}H_{32}O_{16}$	4.459	625.175188	203.0339; 217.0493; 228.0414; 245.0443; 273.0382; 274.0467; 302.0417; 317.0651; 479.1179; 625.1743
5	Ethyl gallate	$\mathrm{C_9H_{10}O_5}$	2.728	395.098669	72.9931;94.3979;107.0508;109.0298;123.0453;134.0371;135.0453;151.0395;179.0352;197.0458
6	Isosalvianolic acid C	$\rm C_{26}H_{20}O_{10}$	5.579	537.102488	72.9932;135.0453;179.0352;197.0457;229.0145;267.066;269.0816;295.0616;339.0518;493.1131
7	5-Hydroxy-7-methoxy-3-(4 hydroxybenzylidene) chroman-4-one	- C ₁₇ H ₁₄ O ₅	6.809	343.082616	117.0345;119.0502;123.0451;135.03;145.0296;151.0402;163.0402;253.0504;297.0402;297.077
8	Yunnaneic acid G	$C_{36}H_{30}O_{16}$	5.981	717.151768	109.0294; 135.0452; 161.0246; 229.0148; 243.0298; 295.0615; 339.0518; 365.0681; 475.1036; 519.0936
9	Malic acid	$C_4H_6O_5$	0.882	133.014146	59.0138;62.2723;71.0139;72.9931;87.0087;88.0404;89.0244;114.9219;115.0036;133.0143
10	N1, N5, N10-(E)-tri-p- coumaroylspermidine	C ₃₄ H ₃₇ N ₃ O	₆ 7.342	584.274149	72.0813;119.0492;147.0438;204.1017;218.1174;275.175;292.2014;420.2275;438.2378;584.2753
11	10-O-Coumaroyl-10-O-deacetylasperuloside	$C_{25}H_{26}O_{12}$	4.811	563.142417	75.0086;89.0243;119.0501;135.0299;163.0402;281.0668;283.0977;327.0877;445.1148;563.1389
12	Nepetin-7-glucoside	$C_{22}H_{22}O_{12}$	4.393	479.117593	203.0338;217.0492;228.0417;245.0443;257.0445;273.0388;274.0467;302.0418;317.0652;479.1172
13	P-Anisic acid	$C_8H_8O_3$	2.354	151.040118	81.0347;95.05;105.0347;108.0217;121.0297;122.0375;123.0452;133.0296;150.0316;151.0402
14	Naringenin 7-O- gentiobioside	$C_{27}H_{32}O_{15}$	4.397	641.176065	125.0244;149.0246;164.0118;256.0375;300.0278;315.0511;475.1461;501.1244;515.1419;641.1764
15	Succinic acid	$C_4H_6O_4$	1.235	117.019188	55.0189;71.0504;73.0295;94.4018;99.0084;99.9258;109.1107;116.0717;116.9285;117.0192
16	Chrysosplenetin	$C_{19}H_{18}O_{8}$	6.954	373.093262	72.9931;123.0453;132.0221;134.0374;135.0453;160.0169;161.0239;175.0404;179.0353;197.0459
17	Salvianolic acid A	$\rm C_{26}H_{22}O_{10}$	5.537	493.11352	72.9931;123.0451;135.0452;179.0352;197.0457;267.0661;269.0817;295.0615;313.0719;493.1139
18	L-Isoleucine	$\mathrm{C_6H_{13}NO_2}$	1.061	132.101714	56.0503;58.0657;69.0705;72.0814;74.0243;84.0451;86.0969;86.1482;87.1001;132.1019
19	Ternatumoside II	$\rm C_{27} H_{30} O_{15}$	5.687	593.152111	135.03; 151.0037; 211.0397; 227.035; 229.0506; 255.0298; 283.0252; 284.0325; 429.084; 593.152
20	Lysofungin	$C_{27}H_{49}O_{12}H_{49}O_{1$	10.141	595.289809	78.959;96.9695;152.9959;223.0017;241.0119;279.233;315.0489;415.2271;433.2367;595.2893
21	Ailanthoidol	$\mathrm{C_{19}H_{18}O_5}$	6.318	361.082629	72.993;123.045;161.0246;179.0352;197.0457;360.08
22	3-Hydroxybenzoic acid	$C_7H_6O_3$	4.747	137.02448	65.0395;73.9387;79.8703;85.1056;93.0345;103.4346;107.8421;136.0167;136.0401;137.0244
23	Isosulochrin	$\mathrm{C_{17}H_{16}O_{7}}$	4.903	377.088166	72.9931;123.0452;135.0452;149.061;179.0344;197.0462;333.0983;347.0778;359.0777;377.0887
24	3-Acetyldeoxynivalenol	$\mathrm{C_{17}H_{22}O_{7}}$	4.842	356.169649	55.0549;83.0496;93.0577;119.0731;120.0809;136.0756;141.0908;220.1329;254.1382;356.1698
25	Neoeriocitrin	${\rm C_{27}H_{32}O_{15}}$	4.853	641.17603	125.0246; 137.0246; 149.0247; 167.0352; 192.0067; 300.0277; 315.0511; 475.1461; 501.1248; 641.1762
26	Caffeic acid	$C_9H_8O_4$	5.112	179.03513	55.7567;59.0138;71.0138;75.0085;89.0244;107.0502;117.0344;134.0375;135.0452;179.0354
27	Clostebol acetate	C ₂₁ H ₂₉ ClO ₃	0.786	401.130389	59.0138;71.0138;85.0294;89.0244;101.0244;113.0243;119.035;161.0458;179.0563;341.1096
28	D-Tryptophan	$C_{11}H_{12}N_2O_2$	2 3.749	203.082668	59.0138;61.8589;72.0091;74.0248;116.0505;130.0665;142.0663;159.0934;186.0562;203.0828
29	Blumeatin B	$\mathrm{C_{17}H_{16}O_{7}}$	5.122	377.088198	72.993;123.0451;133.0295;135.0452;137.0246;161.0246;179.0352;197.0458;359.0778;377.0876
30	Eugenol gentiobioside	$C_{22}H_{32}O_{12}$	5.527	487.181701	59.0138;71.0139;73.0295;89.0244;101.0243;113.0243;161.0457;221.0668;263.0771;445.1722

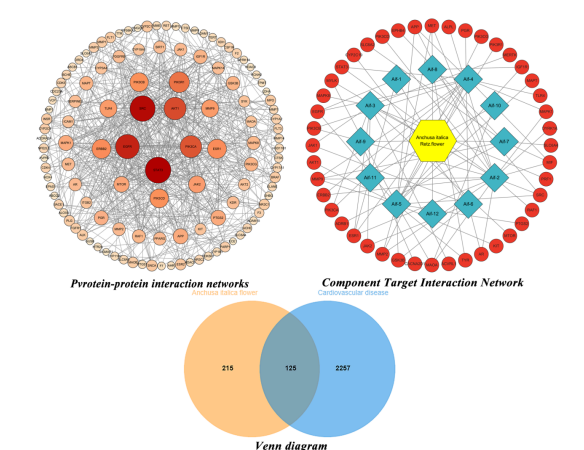


Fig. 1: Network pharmacology-related Venn diagrams, proteininteraction network diagrams, and component-target network diagrams

Table 3: Key Active Ingredients of Anchusa italica Retz. flowers

ID	Metabolite	Pubchem_ID
AIF-1	3-(3,4-Dihydroxyphenyl) lactic acid	439435
AIF-2	5-Hydroxy-7-methoxy-3-(4-hydroxybenzylidene)	15484394
	chroman-4-one	
AIF-3	Ailanthoidol	5316929
AIF-4	Caffeic acid	689043
AIF-5	Chrysosplenetin	5281608
AIF-6	Clostebol acetate	13327
AIF-7	D-Tryptophan	9060
AIF-8	Ethyl gallate	13250

The top 3 active ingredients in the network with the highest degree values were 5-Hydroxy-7-methoxy-3-(4-hydroxybenzylidene) chroman-4-one (degree: 14), Chrysosplenetin (degree: 14), caffeic acid (degree: 12), are the key active ingredients of the network.

Results of GO and Kegg Enrichment Analysis

Go and Kegg analyses were conducted via the microbiology platform, and the analysis module integrated R language packages such as clusterProfiler, pathview, etc. The data were screened with Pvalue ≤ 0.05, and 1,022 BP entries were obtained, which were mainly involved in cellular response to chemical stress, phosphatidylinositol-mediated signaling, protein kinase B signaling, response to oxidative stress and other processes. A total of 68 CC entries were identified, membrane. mainly involving basement cell phosphatidylinositol 3-kinase complex, etc. 115 MF entries were identified, mainly involving phosphatase binding, phosphatidylinositol kinase activity, protein phosphatase binding, etc., and the top 10 entries of each item were imported into the microbiology platform for visualization. The results of GO enrichment analysis are shown in Figure 2. 143 pathways were identified by KEGG screening, the top 20 pathways were enriched and analyzed.

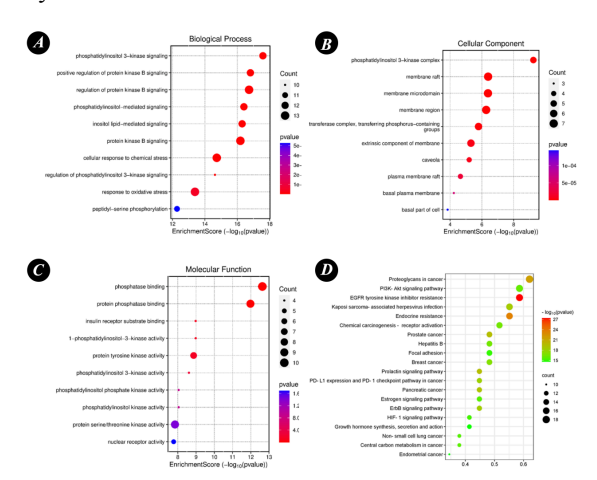


Fig. 2: Results of enrichment analysis (A: Biological Process; B: Cellular Component; C: Molecular Function; D: KEGG enrichment)

Docking of Molecules

The components with the top three-degree values were molecularly docked with the proteins with the top five-degree values, and the protein information is shown in Table 4.

Table 4: Core protein-related information

ID	Uniprot ID	PDB ID	Degree
STAT3	P40763	6NJS	42
SRC	P12931	1FMK	41
EGFR	P00533	1XKK	37
PIK3CA	P42336	7L1C	34
AKT1	Q38998	5AAR	33

STAT3 is a transcription factor that plays a role in myocardial protection and the regulation of myocardial hypertrophy (Yang *et al.*, 2020). It is also involved in a number of cardiovascular physiological and pathological

processes, including cardiomyocyte necrosis, ischemiareperfusion injury, myocardial hypertrophy, and myocardial fibrosis. SRC is a non-receptor-type protein tyrosine kinase that is involved in a variety of cellular processes, including cell proliferation, differentiation, and migration. In the cardiovascular system, SRC has the potential to be involved in the protective and injury responses of cardiomyocytes (Hussain et al., 2023). However, its specific role may depend on the specific pathological conditions under consideration. Activation of EGFR is associated with cardiomyocyte growth and repair. Its role in cardiovascular disease may be doubleedged, and further in-depth studies are required to elucidate its specific mechanisms (Masuda et al., 2023). Aberrant activation or dysfunction of PIK3CA and AKT1 could potentially contribute to the development of cardiovascular disease. PIK3CA affects vascular health through its role in cell signaling, whereas AKT1 is directly involved in physiological and pathological processes in the heart and blood vessels. These findings suggest that PIK3CA and AKT1 may be potential targets for the development of novel therapies for cardiovascular disease (Fang et al., 2019). EGFR has been shown to interact with a variety of molecules, including PIK3CA and AKT1, among others. It is imperative to acknowledge the potential for stimulation or inhibition of these genes to exert a cascading effect on other enzyme activities and molecular pathways. A notable example is the direct phosphorylation of STAT proteins by EGFR. which promotes their dimerization and nuclear translocation, thereby regulating the expression of immune-related genes, such as cytokines. The aforementioned intervention has been demonstrated to impede the process by which tumors evade the immune system, thereby augmenting the sensitivity of the tumors to chemotherapy (Logue & Morrison, 2012). The docking results demonstrated that 5-Hydroxy-7methoxy-3-(4-hydroxybenzylidene) chroman-4-one and caffeic acid (CA) exhibited the most favorable outcomes in terms of their interaction with EGFR and SRC, with docking scores of 99.0153 and 78.7345, respectively. These findings are illustrated in Figures 3 and 4.

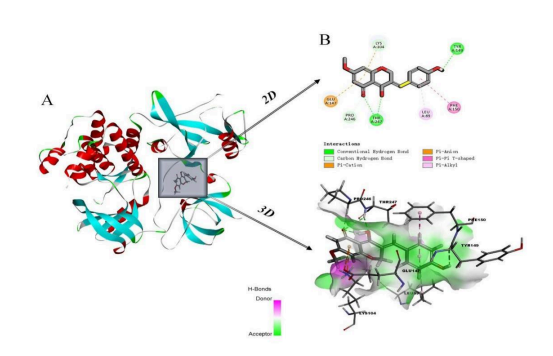


Fig. 3: Docking results for key compounds: 5-Hydroxy-7-methoxy-3-(4-hydroxybenzylidene) chroman-4-one with SRC (A: overall docking results, B: 2D and 3D display of molecule-specific docking points)

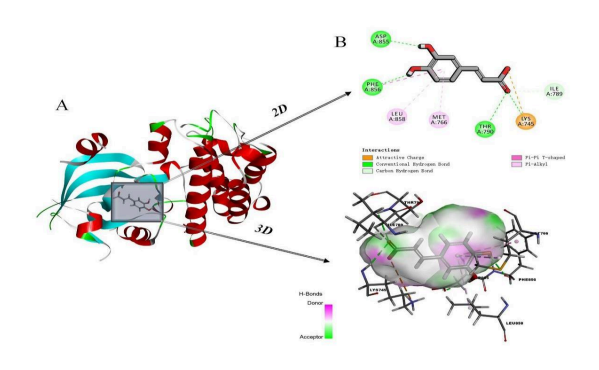


Fig. 4: Docking results for key compounds: Caffeic acid and EGFR (A: overall docking results, B: 2D and 3D display of molecule specific docking sites)

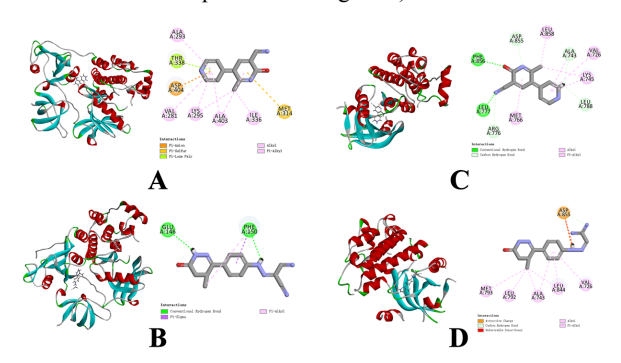


Fig. 5: Molecular docking results of Milrinone and Levosimendan (A: SRC-Milrinone, B: SRC-Levosimendan, C: EGFR-Milrinone, D: EGFR-Levosimendan)

Milrinone is a pharmaceutical agent that functions by inhibiting phosphodiesterase activity, resulting in positive inotropic and vasodilatory effects (Huang et al., 2011). It is a commonly prescribed medication for the treatment of cardiovascular diseases, including heart failure and acute heart failure. Levosimendan is another pharmaceutical agent that is clinically indicated for the treatment of heart failure. In order to perform a comprehensive analysis, molecular docking was utilized to study the interaction between two proteins, SRC and EGFR (Antila et al., 2000). Negative controls were implemented, and the scores of known cardiovascular drugs that interacted with the proteins were compared. In addition, benchmarking of inhibitors was performed. The analysis of their similarities and differences in binding affinity and binding modes can facilitate a more comprehensive understanding of the pharmacological properties of the research molecules and provide significant references for subsequent drug development. The results of the docking are shown in Figure 5. The docking results demonstrated that the highest sitespecific docking scores of Milrinone with SRC and EGFR were 77.7611 and 66.8557, respectively, which were lower than the docking scores of 5-Hydroxy-7methoxy-3-(4-hydroxybenzylidene) chroman-4-one and SRC (99.0153). The highest docking scores of Levosimendan with SRC and EGFR were 101.7991 and

93.9514, respectively, which were higher than those of the target components, suggesting further optimization of the target components. This finding indicates that the target component has the potential to be further optimized as a cardiovascular drug.

Figure 6 illustrates the extent to which the six distinct docking groups exert their influence on the target scoring system. The results indicate that Group A exhibited the highest scores, demonstrating an extremely significant difference (***, p < 0.0001), suggesting a substantial enhancement in the model.Group E demonstrated a highly significant difference (**, p < 0.01), while Group B exhibited statistically significant differences (*, p < 0.05). In contrast, the difference between groups C and D was not statistically significant (ns, $p \ge 0.05$). To a certain extent, these findings suggest that the docking effect of the target component with the inhibitor is difficult and unsatisfactory. All data are expressed as mean \pm standard deviation (mean \pm SD). The significance level was adjusted to account for multiple comparisons using one-way ANOVA, followed by multiple comparisons.

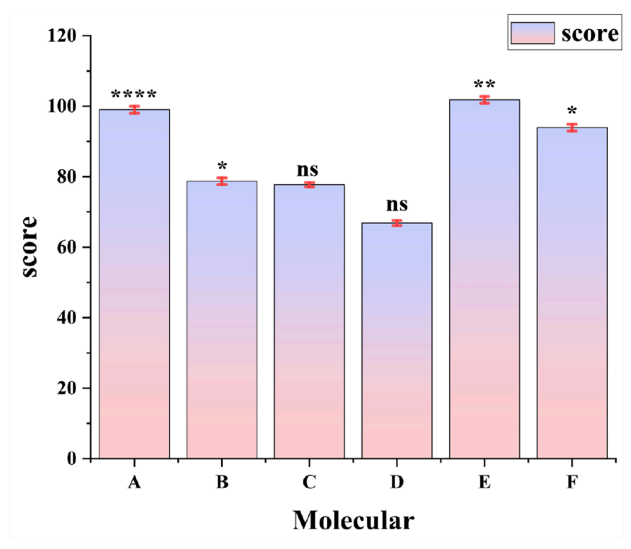


Fig. 6: Molecular docking significance analysis (A: 5-Hydroxy-7-methoxy-3-(4-hydroxybenzylidene) chroman-4-one-SRC); B:Caffeic acid-EGFR; C: SRC-Milrinone; D: EGFR-Milrinone; E: SRC-Levosimendan; F: EGFR-Levosimendan

Molecular Dynamics of Markers for Anchusa italica Retz. flowers

The root-mean-square deviation (RMSD) from the molecular dynamics (MD) simulation serves as a metric for understanding the motion process of the complex. A higher RMSD, coupled with pronounced fluctuations, signifies intense movement, while lower values and steady trends reflect smoother motion. As demonstrated in Figure 7, the STING/Elafibranor complex converges after 40 ns of simulation and fluctuates stably within the range of 3-4 Å. This finding indicates that the small

molecule exhibits a high degree of binding affinity and stability to the protein. The 5-Hydroxy-7-methoxy-3-(4-hydroxybenzylidene) chroman-4-one consent term is HY-N8673 in the Pubchem database.

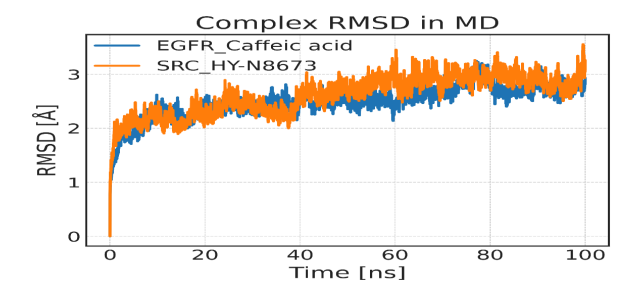


Fig. 7: Root mean square deviation (RMSD) of complexes over time during molecular dynamics simulations

RMSF can respond to the flexibility of the protein during molecular dynamics simulation. Usually, after the drug binds to the protein, the flexibility of the protein decreases, which leads to the stabilisation of the protein and the effect of enzyme activation. As shown in the Figure 8, the RMSF of the protein is within 2Å except for the local region of the protein, which indicates that the main structure of the protein is very rigid, and the effect may be achieved by binding the small molecule Elafibranor.

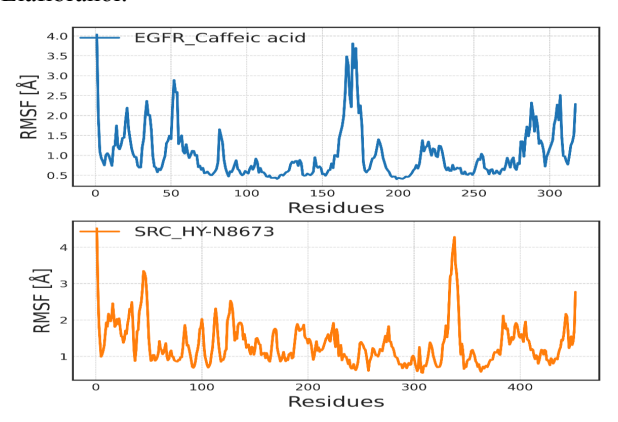


Fig. 8: Root-mean-square fluctuations (RMSF) calculated based on molecular dynamics simulation trajectories

MM-GBSA Binding Free Energy Calculations

The trajectory of molecular dynamics simulation was utilised to calculate the binding energies using the MM-GBSA method, a technique that has been demonstrated to offer enhanced accuracy in reflecting the binding effects of small molecules and target proteins.

As demonstrated in Table 5, the binding energies of EGFR_Caffeic acid and SRC_HY-N8673 were determined to be -32.80±1.40 and -17.40±0.37 kcal/mol, respectively. The negative values thus indicate that these two molecules have binding affinity to the target protein, and lower values indicate stronger binding. The calculations demonstrate that both molecules exhibit a high degree of binding affinity. Energy decomposition

analysis reveals that the primary contributing factor to the binding of EGFR_Caffeic acid, SRC_HY-N8673 is van der Waals energy, followed by electrostatic energy, and then non-polar solvation free energy.

Table 5: Binding free energies and energy components predicted by MM/GBSA (kcal/mol)

System name	EGFR_Caffeic acid	SRC_HY-N8673
$\Delta E_{ m vdw}$	-20.04±2.04	-28.45±1.73
$\Delta E_{ m elec}$	-6.39±6.32	-9.34±2.47
ΔG_{GB}	-2.45±5.75	24.01±3.48
ΔG_{SA}	-3.90±0.19	-3.62±0.24
$\Delta G_{ ext{bind}}$	-32.80±1.40	-17.40±0.37

Using the MM-GBSA energy disaggregation technique, we identified the top 10 amino acids crucial for the binding of EGFR to Caffeic acid, and were THR 854, LYS 745, PHE 856, LEU 858, ASP 855, MET 766, LEU 861, LEU 788, LEU 777, and THR 79. For SRC_HYN8673, the top 10 contributing amino acids are LEU 89, GLU 147, GLY 105, LYS 104, VAL 87, ALA 88, THR 247, TYR 90, GLU 106, and TYR 149, respectively. It can thus be concluded that these amino acids are critical. As shown in Figure 9.

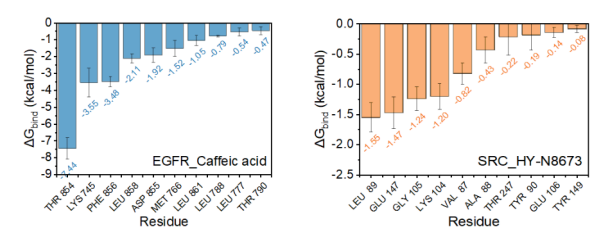


Fig. 9: The Ten Key Amino Acids Critical for Small Molecule and Protein Binding

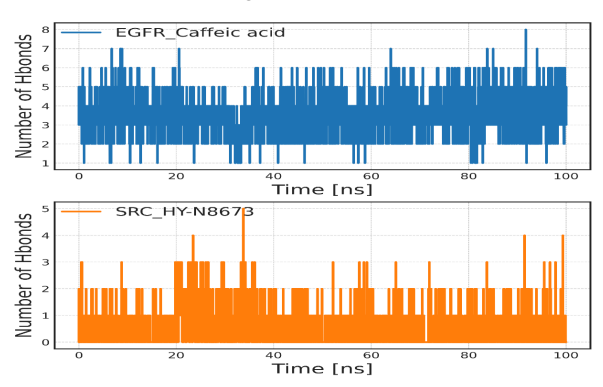


Fig. 10: Changes in the number of hydrogen bonds between small molecules and proteins during molecular dynamics simulations

Hydrogen bonding interaction is one of the strongest non-covalent interactions. In this study, the number of hydrogen bonds formed between ligand molecules and proteins during 100ns molecular dynamics simulations was monitored. As demonstrated in Figure 10, the number of hydrogen bonds formed by EGFR_Caffeic acid and SRC_HY-N8673 during the simulation was distributed between 0-7 and 0-5, with EGFR_Caffeic

acid concentrating on 3-4 most of the time, and SRC_HY-N8673 concentrating on 0 most of the time. This observation suggests that hydrogen bonding interactions play a significant role in the stable binding of EGFR_Caffeic acid and SRC_HY-N8673. It appears that hydrogen bonding strongly influences the binding stability of EGFR_Caffeic acid, while its effect on SRC_HY-N8673 binding is weaker.

ADMET Prediction of Anchusa italica Retz. Flowers

Lipinski's 'Rule of Five' can be used to describe the drug-like properties of small molecules associated with oral bioavailability characteristics, including log P (less than 5), molecular weight (less than 500), number of hydrogen bond donors (less than or equal to 5) and number of acceptors (less than or equal to 10). The results show that both molecules fulfil all the criteria of the Rule of Five. The rosemarinic acid molecule has a relatively large number of eight hydrogen-bonded receptors and low drug similarity. In addition to the druglike properties, the ADMET properties of the molecules were predicted. The Caco-2 values for molecules HY-N8673, caffeic acid, and rosmarinic acid were -4.917, -4.94, and -6.513, respectively, suggesting that HY-N8673 and caffeic acid have higher permeability to membranes, while rosmarinic acid has lower permeability. Additionally, the Pgp-substrate probability was all less than 0.1, indicating that all three molecules have a low probability of being exocytosed after entering

The plasma protein binding of HY-N8673, caffeic acid and rosmarinic acid was determined to be 95.41%, 64.67% and 77.28%, respectively. This suggests that HY-N8673 exhibits high plasma protein binding, while caffeic acid and rosmarinic acid demonstrate lower binding affinities. Furthermore, the volume distribution of the three molecules was found to be minimal, suggesting that their distribution characteristics in vivo are inadequate, thus preventing the molecules from crossing the blood-brain barrier. The half-life of the HY-N8673 molecule was found to be more segmented at 0.832 h, that of caffeic acid at 2.07 h, and that of rosmarinic acid at 1.906 h.

Furthermore, the clearance rates of the two drugs, HY-N8673, and rosmarinic acid, were 7.495, 14.358, and 13.238 mL/min/kg, respectively. These clearance rates are moderate.

It has been shown that rosmarinic acid with more favorable ADMET prediction can be used as a potent antiviral source for the development of drugs for the treatment of SARS-CoV-2 infection (Patel *et al.*, 2023). Caffeic acid is also more abundantly studied, with studies of ADMET prediction and molecular docking of caffeic acid showing the ability to inhibit HMGCR, which provides cholesterol-lowering potential (Heera *et al.*, 2022). Finally, a prediction of the toxicity of the

molecules was made. The prediction indicated that HY-N8673, caffeic acid, and rosmarinic acid did not demonstrate hERG toxicity; HY-N8673 and rosmarinic acid may exhibit Ames mutagenesis toxicity, while caffeic acid did not manifest Ames mutagenesis toxicity.

Discussion

A network pharmacological study was conducted, utilising the UPLC-Q-Exactive Orbitrap-MS data. The construction of the 'active ingredient-target gene' network resulted in the identification of 28 core targets, which were subjected to further analysis. The primary markers identified by web-based pharmacological screening included HY-N8673 and caffeic acid, among other compounds. Prior studies utilising UPLC-Q-Exactive Orbitrap-MS analysis have demonstrated that the relative abundance of rosmarinic acid in Airfs can reach up to 39.8511%, with notable concentrations also observed for CA and 3,4-Dihydroxyphenyllactic acid (Wang et al., 2024). These findings suggest that rosmarinic acid is a natural phenolic acid derived from the esterification of CA and 3,4-Dihydroxyphenyllactic acid (Noor et al., 2022). The structural relationship between the two compounds enables rosemarinic acid to inherit a number of the bioactive properties of caffeic acid, including antioxidant, anti-inflammatory and antibacterial properties (Takeda et al., 2002). This partially elucidates the indirect role played by this substance, rosemarinic acid, in the prevention of cardiovascular diseases. Research has demonstrated that rosmarinic acid can form complexes with cyclodextrin (CD) derivatives, thereby enhancing its solubility and permeability. For instance, the complex formed with hydroxypropyl-γ-CD (HP-γ-CD) increased permeability from 6.901 \times 10-7 cm/s to 1.085 \times 10-6 cm/s at pH 4.5, which approaches the optimal permeability level. Furthermore, the antioxidant and enzyme inhibitory activities were enhanced. The therapeutic potential of rosemarinic acid can be enhanced by increasing the permeability (Woottisin et al., 2022). Therefore, molecular dynamics simulation was utilised to calculate the binding effect of caffeic acid on target proteins. Subsequently, ADMET was employed to predict its molecular properties and molecular toxicity. The results demonstrated that rosemarinic acid analogues exhibited suboptimal drug properties and membrane permeability, while caffeic acid exhibited favourable drug-forming and absorption properties, a low probability of drug-drug interactions, and an absence of Ames mutagenesis and hERG toxicity (Banerjee & Roy, 2023; Imray & Macphee, 1981). However, it is worth noting that HY-N8673 may be an inhibitor of several metabolic enzymes and there is a risk of drug-drug interactions. HY-N8673 is a member of the flavonoid family, exhibiting notable biological activities, including antioxidant, anti-inflammatory, and anticancer properties. It has been postulated that the compound's ability to bind to metabolic enzymes may result in the inhibition of key enzymes, thereby impacting metabolic pathways. For

instance, the potential for COX-2 (cyclooxygenase-2) inhibition has been suggested, contributing to its anti-inflammatory effects (Li *et al.*, 2024).

Despite the notable efficacy of existing therapeutic agents in the treatment of cardiovascular disease, such as β -blockers, ACE inhibitors, and calcium channel blockers, these medications are limited in their capacity to address the multifaceted pathological mechanisms underlying the condition. They are typically designed to target a single pathway or mechanism, which often results in inadequate therapeutic outcomes and limited improvements in patient prognosis.

Conclusion

In this study, we integrated network pharmacology, molecular docking, and ADMET prediction to screen multiple molecular targets (e.g., STAT3, EGFR, PIK3CA, etc.) associated with cardiovascular diseases. These targets are implicated in various pathological processes, including inflammation, fibrosis, apoptosis. The utilization of multi-target regulation holds great promise in comprehensively intervening in the pathological mechanisms underlying cardiovascular diseases. A comparison with existing therapeutic modalities reveals that the molecular targets and potential drugs identified in this study may offer enhanced precision and the capacity to target specific pathological processes, thereby enhancing therapeutic efficacy and reducing adverse effects.

Authors Contributions

Linyang Wang: Conceptualization, Methodology, Writing - Original Draft, Writing - Review & Editing.

Yan Chen: Methodology.

Ainiwaer Aikemu: Funding Acquisition.

Shuge Tian: Supervision, Writing - Review & Editing.

Funding Information

This study was funded by the Xinjiang Key Laboratory of Hetian Characteristic Chinese Traditional Medicine Research Project (2024-0301) and the Xinjiang Medical University Joint University-Enterprise Project (020823007).

Acknowledgment

We sincerely thank the Xinjiang Key Laboratory of Hetian Characteristic Chinese Traditional Medicine Research for providing financial support for this study (2024-0301), which was also supported by the Xinjiang Medical University Joint University-Enterprise Project (020823007).

Data Availability

Data will be made available on request.

Abbreviations

Airfs, *Anchusa italica* Retz. Flowers; RA, Rosmarinic acid; CA, caffeic acid; HY-N8673, 5-Hydroxy-7-methoxy-3-(4-hydroxybenzylidene) chroman-4-one.

Ethics

This article is original and contains unpublished material. The corresponding author confirms that all of the other authors have read and approved the manuscript and that no ethical issues are involved.

References

Antila, S., Jarvinen, A., Honkanen, T., & Lehtonen, L. (2000). Pharmacokinetic and pharmacodynamic interactions between the novel calcium sensitiser levosimendan and warfarin. *European Journal of Clinical Pharmacology*, *56*(9–10), 705–710. https://doi.org/10.1007/s002280000204

Banerjee, A., & Roy, K. (2023). Machine-learning-based similarity meets traditional QSAR: "q-RASAR" for the enhancement of the external predictivity and detection of prediction confidence outliers in an hERG toxicity dataset. *Chemometrics and Intelligent Laboratory Systems*, 237, 104829. https://doi.org/10.1016/j.chemolab.2023.104829

Chen, K.-K., Xie, Z.-J., Dai, W., & Wang, Q. (2017). A new oleanolic-type triterpene glycoside from *Anchusa italica*. *Natural Product Research*, *31*(8), 959–965.

https://doi.org/10.1080/14786419.2016.1258557

Fang, W., Huang, Y., Gan, J., Yang, Y., Wu, Y., Huang, J., Xu, Z., Wang, W., & Zhang, L. (2019). Abstract 327: The impact of PIK3CA/PTEN/AKT1 genes in advanced NSCLC patients with acquired EGFR-TKI resistance and clinical response to EGFR-TKI plus everolimus combination therapy. *Cancer Research*, 79(13_Supplement), 327–327. https://doi.org/10.1158/1538-7445.am2019-327

Gajera, H. P., Hirpara, D. G., Gevariya, S. N., Savaliya, D. D., & Parasana, J. S. (2024). Exploring the antioxidant and antidiabetic potentials of *Syzygium cumini* L. landraces: phytochemicals, bioactive constituents and pathway enrichment analysis. *International Journal of Food Science and Technology*, 59(8), 5818–5828. https://doi.org/10.1111/ijfs.17337

Genheden, S., & Ryde, U. (2015). The MM/PBSA and MM/GBSA methods to estimate ligand-binding affinities. *Expert Opinion on Drug Discovery*, 10(5), 449–461.

https://doi.org/10.1517/17460441.2015.1032936

Gong, Y., Yang, D., Barrett, H., Sun, J., & Peng, H. (2023). Building the Environmental Chemical-Protein Interaction Network (eCPIN): An Exposome-Wide Strategy for Bioactive Chemical Contaminant Identification. *Environmental Science & Technology*, *57*(9), 3486–3495. https://doi.org/10.1021/acs.est.2c02751

- Heera, R., Chandra, K., Karishma, S., Anita, S., Jaykaran, C., Paras, S., Rajsekhar, R., & Surajit, G. (2022). In-vitro and in-silico determinations of HMG-CoA reductase inhibition potential of caffeic acid for therapeutics of hypercholesterolemia. *Journal of Applied Pharmaceutical Science*. https://doi.org/10.7324/japs.2021.120119
- Hu, B.-C., Liu, Y., Zheng, M.-Z., Zhang, R.-Y., Li, M.-X., Bao, F.-Y., Li, H., & Chen, L.-X. (2020). Triterpenoids from Anchusa italica and their protective effects on hypoxia/reoxygenation induced cardiomyocytes injury. *Bioorganic Chemistry*, 97, 103714.

https://doi.org/10.1016/j.bioorg.2020.103714

- Huang, M.-H., Wu, Y., Nguyen, V., Rastogi, S., McConnell, B. K., Wijaya, C., Uretsky, B. F., Poh, K.-K., Tan, H.-C., & Fujise, K. (2011). Heart Protection by Combination Therapy with Esmolol and Milrinone at Late-Ischemia and Early Reperfusion. *Cardiovascular Drugs and Therapy*, 25(3), 223–232.
 - https://doi.org/10.1007/s10557-011-6302-z
- Hussain, M., Ikram, W., & Ikram, U. (2023). Role of c-Src and reactive oxygen species in cardiovascular diseases. *Molecular Genetics and Genomics*, 298(2), 315–328. https://doi.org/10.1007/s00438-023-01992-9
- Imray, F. P., & Macphee, D. G. (1981). Mutagenesis by Ionizing Radiation in Strains of Salmonella Typhimurium Used in the Ames Test. *International Journal of Radiation Biology and Related Studies in Physics, Chemistry and Medicine*, 40(1), 111–115.
 - https://doi.org/10.1080/rab.40.1.111.115
- Jiang, L., Zhang, W., Wang, B., Cai, Y., Qin, X., Zhao, W., Ji, P., Yuan, Z., Wei, Y., & Yao, W. (2024).
 Exploration of the Potential Mechanism of Yujin Powder Treating Dampness-heat Diarrhea by Integrating UPLC-MS/MS and Network Pharmacology Prediction. Combinatorial Chemistry & High Throughput Screening, 27(10), 1466–1479.
 https://doi.org/10.2174/0113862073246096230926 045428
- Khomsi, M. E., Imtara, H., Kara, M., Hmamou, A., Assouguem, A., Bourkhiss, B., Tarayrah, M., AlZain, M. N., Alzamel, N. M., Noman, O., & Hmouni, D. (2022). Antimicrobial and Antioxidant Properties of Total Polyphenols of Anchusa italica Retz. *Molecules*, 27(2), 416.
 - https://doi.org/10.3390/molecules27020416
- Kräutler, V., van Gunsteren, W. F., & Hünenberger, P. H. (2001). A fast SHAKE algorithm to solve distance constraint equations for small molecules in molecular dynamics simulations. *Journal of Computational Chemistry*, 22(5), 501–508. https://doi.org/10.1002/1096-
 - 987x(20010415)22:5<501::aid-jcc1021>3.0.co;2-v

- Li, W., Jiang, H., Zhang, W., Sun, Q., Zhang, Q., Xu, J., Huang, J., & Wan, Y. (2024). Mechanisms of action of Sappan lignum for prostate cancer treatment: network pharmacology, molecular docking and experimental validation. *Frontiers in Pharmacology*, 15. https://doi.org/10.3389/fphar.2024.1407525
- Linse, J.-B., & Hub, J. S. (2021). Three- and four-site models for heavy water: SPC/E-HW, TIP3P-HW, and TIP4P/2005-HW. *Journal of Chemical Physics*, 154(19), 194501.

https://doi.org/10.1063/5.0050841

- Liu, Z., Ran, Q., Luo, J., Shen, Q., Zhang, T., Fang, S., Pan, K., & Long, L. (2024). Correlation analysis of secondary metabolites and disease resistance activity of different varieties of Congou black tea based on LC-MS/MS and TCMSP. *Food Chemistry: X, 23,* 101331. https://doi.org/10.1016/j.fochx.2024.101331
- Logue, J. S., & Morrison, D. K. (2012). Complexity in the signaling network: insights from the use of targeted inhibitors in cancer therapy. *Genes & Development*, 26(7), 641–650. https://doi.org/10.1101/gad.186965.112
- Lohit, N., Singh, A. K., Kumar, A., Singh, H., Yadav, J. P., Singh, K., & Kumar, P. (2024). Description and *In silico* ADME Studies of US-FDA Approved Drugs or Drugs under Clinical Trial which Violate the Lipinski's Rule of 5. *Letters in Drug Design & Discovery*, 21(8), 1334–1358. https://doi.org/10.2174/1570180820666230224112 505
- Masuda, S., Hara, T., Yamagami, H., Mitsui, Y., Kurahashi, K., Yoshida, S., Harada, T., Otoda, T., Yuasa, T., Nakamura, S., Kuroda, A., Endo, I., Matsumoto, T., Matsuhisa, M., Abe, M., & Aihara, K. (2023). Vascular Endothelial Function Is Associated with eGFR Slope in Female and Non-Smoking Male Individuals with Cardiovascular Risk Factors: A Pilot Study on the Predictive Value of FMD for Renal Prognosis. *Journal of Atherosclerosis and Thrombosis*, 30(11), 1727–1741. https://doi.org/10.5551/jat.63987
- Murugan, R., Tamil Selvan, S., Dharmalingam Jothinathan, M. K., Srinivasan, G. P., Rajan Renuka, R., & Prasad, M. (2024). Molecular Docking and Absorption, Distribution, Metabolism, and Excretion (ADME) Analysis: Examining the Binding Modes and Affinities of Myricetin With Insulin Receptor, Glycogen Synthase Kinase, and Glucokinase. *Cureus*.
 - https://doi.org/10.7759/cureus.53810
- Nguyen, H., Roe, D. R., & Simmerling, C. (2013). Improved Generalized Born Solvent Model Parameters for Protein Simulations. *Journal of Chemical Theory and Computation*, 9(4), 2020–2034
 - https://doi.org/10.1021/ct3010485

- Noor, S., Mohammad, T., Rub, M. A., Raza, A., Azum, N., Yadav, D. K., Hassan, M. I., & Asiri, A. M. (2022). Biomedical features and therapeutic potential of rosmarinic acid. *Archives of Pharmacal Research*, *45*(4), 205–228. https://doi.org/10.1007/s12272-022-01378-2
- Patel, U., Desai, K., Dabhi, R. C., Maru, J. J., & Shrivastav, P. S. (2023). Bioprospecting phytochemicals of Rosmarinus officinalis L. for targeting SARS-CoV-2 main protease (Mpro): a computational study. *Journal of Molecular Modeling*, 29(5). https://doi.org/10.1007/s00894-023-05569-6
- Rastelli, G., Rio, A. D., Degliesposti, G., & Sgobba, M. (2010). Fast and accurate predictions of binding free energies using MM-PBSA and MM-GBSA. *Journal of Computational Chemistry*, 31(4), 797–810. https://doi.org/10.1002/jcc.21372
- Salomon-Ferrer, R., Case, D. A., & Walker, R. C. (2013). An overview of the Amber biomolecular simulation package. *WIREs Computational Molecular Science*, *3*(2), 198–210. https://doi.org/10.1002/wcms.1121
- Santos, E. M. S., Santos, H. O., Martins, E. R., Da Fonseca, F. S. A., Aguilar, C. M., Pereira, U. A., Junior, N. N., Gomes, M. S., De Souza, C. N., Ravnjak, J. M. A., Porto, R. R., & De Almeida, A. C. (2022). Protein-coding gene interaction network prediction of bioactive plant compound action against SARS-CoV-2: a novel hypothesis using bioinformatics analysis. *Anais Da Academia Brasileira de Ciências*, 94(suppl 3), 1–23. https://doi.org/10.1590/0001-3765202220201380
- Shu, X., Ye, L., Han, S., Liang, L., Song, H., Xue, S., Zhao, Y., Ling, S., & Liu, B. (2024). Investigation of the Active Ingredients and Mechanism of Action of YGZ223 in the Treatment of Senile Pruritus Using Network Pharmacology and UPLC-MS. *Natural Product Communications*, *19*(10). https://doi.org/10.1177/1934578x241261015
- Takeda, H., Tsuji, M., Inazu, M., Egashira, T., & Matsumiya, T. (2002). Rosmarinic acid and caffeic acid produce antidepressive-like effect in the forced swimming test in mice. *European Journal of Pharmacology*, 449(3), 261–267. https://doi.org/10.1016/s0014-2999(02)02037-x
- Wang, J., Wolf, R. M., Caldwell, J. W., Kollman, P. A., & Case, D. A. (2005). Junmei Wang, Romain M. Wolf, James W. Caldwell, Peter A. Kollman, and David A. Case, "Development and testing of a general amber force field" *Journal of Computational Chemistry* (2004) 25(9) 1157–1174. *Journal of Computational Chemistry*, 26(1), 114–114.
 - https://doi.org/10.1002/jcc.20145

- Wang, L., Chen, P., Aikemu, A., Zhang, H., & Tian, S. (2024). Study on ultrasonic-assisted deep eutectic solvent extraction process and in vitro antioxidant of Anchusa italica Retz. Flowers. *Ultrasonics Sonochemistry*, 111, 107127. https://doi.org/10.1016/j.ultsonch.2024.107127
- Woottisin, N., Sukprasert, S., Kulsirirat, T., Tharavanij, T., & Sathirakul, K. (2022). Evaluation of the Intestinal Permeability of Rosmarinic Acid from Thunbergia laurifolia Leaf Water Extract in a Caco-2 Cell Model. *Molecules*, *27*(12), 3884. https://doi.org/10.3390/molecules27123884
- Xiang, Z., Guan, H., Zhao, X., Xie, Q., Hu, X., Liu, W., Sun, X., Zhang, S., Li, M., & Wang, C. (2024). Characterization of active alkaloids and metabolites in rats after oral administration of Zuojin Pill using UHPLC-Q-TOF-MS combined with bioinformatics and molecular docking analyses. *Journal of Pharmaceutical and Biomedical Analysis*, 249, 116340.
 - https://doi.org/10.1016/j.jpba.2024.116340
- Xiong, G., Wu, Z., Yi, J., Fu, L., Yang, Z., Hsieh, C., Yin, M., Zeng, X., Wu, C., Lu, A., Chen, X., Hou, T., & Cao, D. (2021). ADMETlab 2.0: an integrated online platform for accurate and comprehensive predictions of ADMET properties. *Nucleic Acids Research*, 49(W1), W5–W14. https://doi.org/10.1093/nar/gkab255
- Xu, L., Sun, H., Li, Y., Wang, J., & Hou, T. (2013). Assessing the Performance of MM/PBSA and MM/GBSA Methods. 3. The Impact of Force Fields and Ligand Charge Models. *The Journal of Physical Chemistry B*, *117*(28), 8408–8421. https://doi.org/10.1021/jp404160y
- Yang, D., Fan, D., Yang, Z., & Tang, Q. Z. (2020). Research progress on the role of STAT3 in cardiovascular diseases. *Zhonghua Xin Xue Guan Bing Za Zhi*, 48(7), 616–620. https://doi.org/10.3760/cma.j.cn112148-20190807-00469